Optical Photon Counting Imaging Detectors with Nanosecond Time Resolution for Astronomy and Night Time Sensing

Oswald H.W. Siegmund, John V. Vallerga, Anton Tremsin, Jason McPhate, Barry Welsh
Space Sciences Laboratory, U.C. Berkeley

ABSTRACT

Microchannel plate photon counting, imaging sensors with cross strip readouts having 18 mm active area format in sealed tube (optical sensing) configurations have been constructed. These have been tested with custom high-speed field programmable gate array based electronics for single event position and time encoding. The Super-GenII photocathodes used have response from 400 nm to 900 nm and peak quantum efficiency of between 16% and 19% at 500 nm. This sensor system achieves spatial resolution of ~30 µm FHWM (at gains of ~ 10^6). The encoding electronics can process high event rates (> 6 MHz input rates), and has event timing accuracy of better than ~1 ns. Local area counting rates of up to 40 kHz (100 µm spot) have been attained and image linearity and stability are better than 50 µm.

Keywords: Microchannel plate, photon counting, imaging, timing

1. INTRODUCTION

Astronomical [1-6] and remote sensing applications [7] have specific sensor requirements that can be addressed well with microchannel plate (MCP) based photon counting, imaging, time stamping detector schemes. We have developed a new generation of detectors using the Cross Strip (XS) anode readout for MCPs that have some significant performance characteristics for these applications. Other prospective uses include time resolved biological imaging [8, 9] and photoelectron emission spectroscopy [10].

The XS readout anode detects microchannel plate charge signals on two orthogonal layers of strips and uses this charge division and centroiding of the charge distribution to encode event X-Y positions, and event times. A depiction of an XS detector scheme is shown in Fig. 1. For a sealed tube device the radiation passes through the input window and is converted to photoelectrons by a photocathode. The emitted photoelectrons are amplified by a pair of MCPs and are detected by the cross strip anode. Initial tests were done with open face schemes appropriate for use in short wavelength and particle detection applications. Subsequently a sealed tube configuration with a proximity focus Super-GenII photocathode for visible light sensing was constructed. Our development of the XS anode scheme has employed XS detectors with active areas of 18 mm using pairs of 6 micron pore microchannel plates. The gain required for XS readouts is ~10^6, an order of magnitude lower than many other high resolution readouts. This substantially increases the overall detector lifetime and the local counting rate capability.

Encoding electronics for the XS detectors has also been built to determine event positions and times. Multi-channel preamplifier ASICs with 32 channels have been implemented on front end boards. The pre-amplified XS anode signals are then sent to a parallel channel encoding system. The latter uses 12 bit ADCs that digitize the signal at 50 Msps and FPGA firmware has been implemented for digital peak detection and subsequent event centroid position and time of arrival calculation. This Parallel Cross Strip (PXS) electronics has allowed us to demonstrate 18mm sealed tube XS detectors with high spatial resolution (~ 30 microns FWHM), input event rates of > 6 MHz and event timing of ~1 ns. Using the PXS electronics scheme and Super-GenII sealed tubes we have demonstrated good spatial image linearity and high local counting rate capability (> 40 KHz /100µm spot) using low MCP gain (5 x 10^5). Background rates are dominated by the thermionic noise of the red sensitive photocathodes, but can be brought down to < 6 kHz at 15°C.

Imaging photon counting MCP detectors have already been used for a number of applications including biological fluorescence lifetime imaging [9], neutron imaging [12], and space based instruments [11]. Detector systems using the developments of XS readout described here may be a significant improvement for several important applications, including airborne and space situational awareness, and astronomy of transient and time-variable sources.

A demonstration of the potential for XS MCP sealed tube detectors is illustrated by the application of an earlier generation of a similar detector at the SAAO SALT 10m telescope. It is engaged in a variety of observations of transient and variable astronomical objects with event time tagging to better than 25 ns, and is able to detect and image faint meteors as they cross the field of view.

2. CROSS STRIP DETECTOR SYSTEMS

2.1 Cross Strip – Microchannel Plate Detector Scheme

Photon event detection, with determination of the centroid of an electron cloud after its multiplication by microchannel plate(s), can be a very effective way of registering events to high spatial and temporal accuracy. We have implemented the XS anode as a multi-layer metal and ceramic structure on an alumina substrate (Fig. 2). The substrate has strip conductors on a ~0.6 mm period applied first. Then sets of insulating and conducting fingers are applied in the orthogonal direction, but ensuring that 50 % of the bottom layer is left exposed so that top and bottom strip conductors collect the charge from the MCPs with equal charge sharing between the axes. The crosstalk between axes is kept small by including ground strips between the upper and lower sense strip layers. The materials used to construct XS anodes in this way have low outgassing, and accommodate >800°C temperatures, making them compatible with sealed tube ultra high vacuum devices. The XS anodes are spaced ~2.5 mm behind the MCP stack and each strip signal is connected through a hermetic via to the back of the anode. A fan out (Fig. 4) outside the vacuum is implemented to accommodate a standard connector for the electronics. The MCP charge cloud is adjusted using a MCP-anode gap voltage so that charge is collected on several neighboring fingers (Fig. 1) to ensure an accurate event centroid can be determined [13]. Two MCPs provide sufficient electron gain (~ 10^6) for high resolution imaging with XS anodes. XS anode sizes of 32 x 32 mm, 50 x 50 mm square formats [13, 14] and 22mm round format have been tested in open face laboratory detectors that have demonstrated excellent resolution (<7 μm FWHM) at low MCP gain (~5 x 10^5) [13].

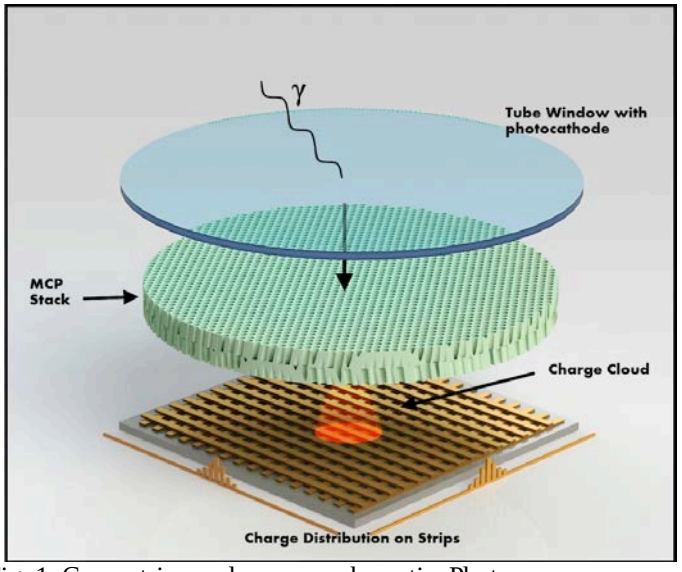

Fig. 1. Cross strip anode sensor schematic. Photons are converted by a photocathode deposited on the window facing a pair of MCPs. The photo-electrons are multiplied by MCPs and are collected by several strips in each axis of the anode.

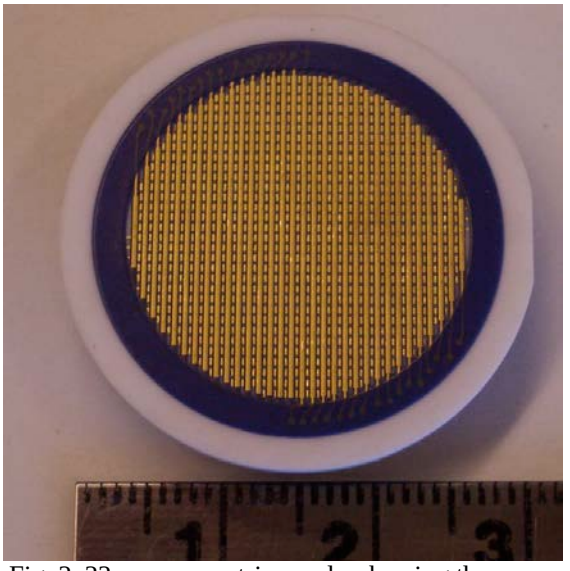

Fig. 2. 22 mm cross strip anode, showing the upper lower strips, which each collect ~50% of the incident charge. Through hole vias transfer the signals to the back side for connections to the amplifiers (Fig. 4).

2.2 Sealed Tube Cross Strip Anode Microchannel Plate Sensors

Development of XS readouts for microchannel plate detectors began [11, 15, 16] with the implementation of open face devices for UV detection in a vacuum environment. To apply these devices to optical photon sensing we have built sealed tubes (Fig. 3) with PHOTONIS. The 22mm XS anode design (Fig. 2) is being used in both open face and in these sealed tube MCP devices. The XS anode is brazed to the back of the tube assembly with an anode to MCP distance of ~2.5mm. A borosilicate glass entrance window is used, with a Super-GenII photocathode which is proximity focused (<200 μm gap, ~ 100 Vgap) to the input of a pair of MCPs. The Super-GenII photocathodes (Fig. 8) that were deposited by Photonis during tube fabrication are modified multialkali photocathodes with redder response than the standard multialkali photocathodes. One consequence of this extended response is higher photoemissive noise which varies with the long wavelength cutoff efficiency profile. The sealed tube with the shortest cutoff has a thermionic background rate of ~14 kHz cm^{-2} at 25 °C. However, without active cooling this drops to ~2.5 kHz cm^{-2} at 15 °C so in many applications Peltier or other cooling methods are not required. The MCP pair is placed `back to back' and each MCP has 6μm pores, 80:1 pore length to diameter ratio (L/d), and a 12 degree pore bias angle. We have used a relatively low acceleration voltage (~100 V) for the anode gap, which is sufficient to establish the required charge

cloud footprint. High local event counting rates can be accommodated [16] since the MCPs used for these tubes are relatively low resistance (<50 MΩ). A final step after the sealed tube is made, is to attach the connector (Fig. 4) to allow connection of the preamplifier board (Fig. 7). The new 18mm sealed tube XS sensors described here are being used for applications in night-time remote sensing [16] and ground based astronomy [6]. It may also be possible to employ GaAs and GaAsP photocathodes in similar sealed tubes in the future giving significantly increased efficiency.

Fig. 3. 18 mm sealed tube sensor using the 22 mm cross strip anode shown in Fig. 2. The tube has a SuperGen-II photocathode giving a broad wavelength range coverage.

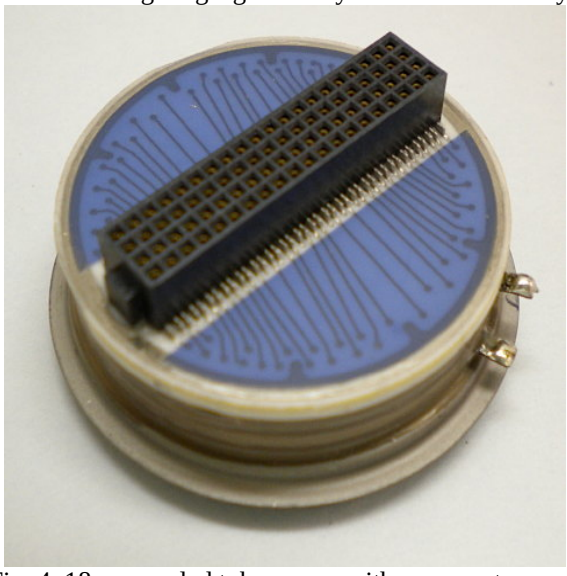

Fig. 4. 18 mm sealed tube sensor with a connector attached to the strip signals routed from the front of the anode. This is attached to the amplifiers (Fig.7).

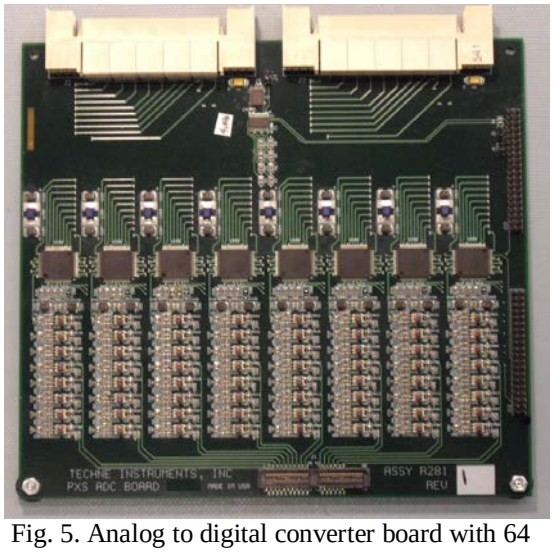

Fig. 5. Analog to digital converter board with 64 channels using octal 65 MHz 12 bit ADC chips for the amplified signals from the X and Y (32 +32 channel) RD20 ASICs coupled to the cross strip anode (Fig. 7).

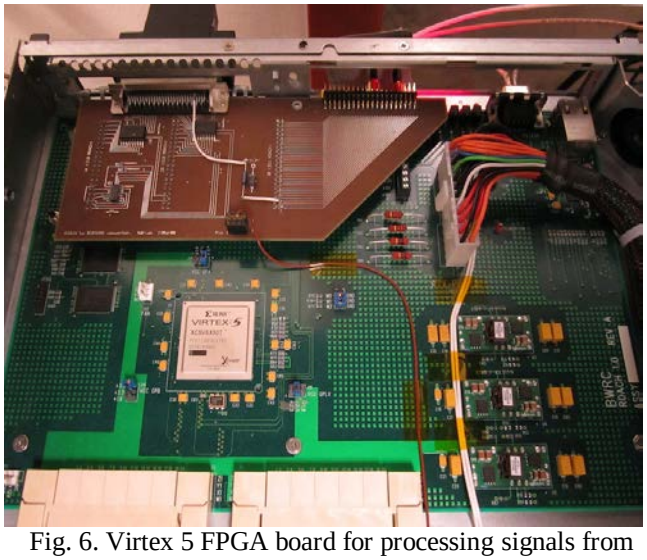

Fig. 6. Virtex 5 FPGA board for processing signals from the digitized amplifier outputs of the cross strip sensor. Firmware makes data corrections, and outputs event positions and times to a PC for storage and display.

2.3 Cross Strip Sensor Image and Time Encoding Electronics

The XS anode pattern is spatially coarse, so determination of event positions on XS anodes requires the electronics to process event signals and calculate the centroids of the electron charge cloud distributions [17] to much better than the anode period [18]. The parallel cross strip electronics (PXS) scheme that we have developed begins with anode strip signal (32 X and 32 Y for the 22 mm XS anode) amplification on 32 channel ASICs (preshape-32, RD20 from Rutherford Appleton Laboratory and Imperial College London). Two RD-20 ASICs are used on each preamplifier board (Fig. 7) [16] to accommodate 64 channels per board. The output signals have ~40 ns rise time, and ~250 ns fall time (gain ~0.7 mV/1000 e^-) and the noise is <1500 electrons rms when attached to the 22 mm cross strip anodes (Fig.

4). The amplified signals are buffered and transferred via a <2 m cable to an ADC board (Fig. 5) where they are digitized by 12 bit analog to digital converters (ADCs, Analog Devices ADS5272) operated at 50 MHz sample rate. The 64 digital sample streams are then transferred to an FPGA (Xilinx Virtex5) board (Fig. 6) using a LVDS serial transfer at 300MHz. All the event data filtering and processing is accommodated in the FPGA allowing us maximum flexibility in signal algorithms. Custom firmware filters are used to determine the peak charge [18] on the group of neighboring strips affected by an incident event, and corrections are applied to the data to account for amplifier gain variations, gain non-linearities, signal offsets and pedestals. Event processing begins when the signal on one or several channels exceeds the predetermined slew threshold, thus establishing a self-triggered configuration. The set of digitized values from the triggered strip channels is passed to the FPGA-peak detection logic. The accuracy of peak detection is improved by filtering the digitized waveforms with "finite impulse response" (FIR) filtering [19]. This is a pipeline process, where earlier samples are retained until clocked out of the algorithm. Event processing algorithms use the output of the digital filters to calculate the peak value of the digitized signal and its temporal position and store the 64 outputs at event rates up to 10 MHz. The timing of the event can be calculated to better than 1 ns accuracy with digital implementation of interpolating algorithms (digital Constant Fraction Discrimination). The event data are then buffered before being transferred to a computer as an event list of X, Y and T. A daughterboard interface is also used to accommodate parallel data transmission of the event data to a standard PCI digital interface.

2.4 Cross Strip Detector System Imaging Tests

We have evaluated the imaging performance of sealed tube 18mm sensors combined with the electronics, consisting of the PXS and the RD20 amplifier board attached. Measurement of the spatial resolution and image linearity is conveniently accomplished by projecting a test mask image with small (10 μm) pinholes at regular intervals (1 mm) onto the photocathode plane (Fig. 9). The image linearity is stable and shows very little distortion. The areas close to edge of the field of view show evidence of some displacement, however, as a result of field fringing caused by the MCP support ring. The spatial resolution is evaluated by measuring the width of the spot images in Fig. 9. The spatial resolution as a function of MCP gain is shown in Fig. 10. At the highest gain (~ 10^6 e^-) the resolution is ~32 μm FWHM. Slightly better resolution (~ 25 μm FWHM) was achieved for events originating at the surface of the top MCP from a hotspot (dust particle). We conclude that the cathode proximity gap/potential is a significant contributor to the spatial resolution achieved. This contribution can be reduced by increasing the proximity gap potential (now ~100 V).

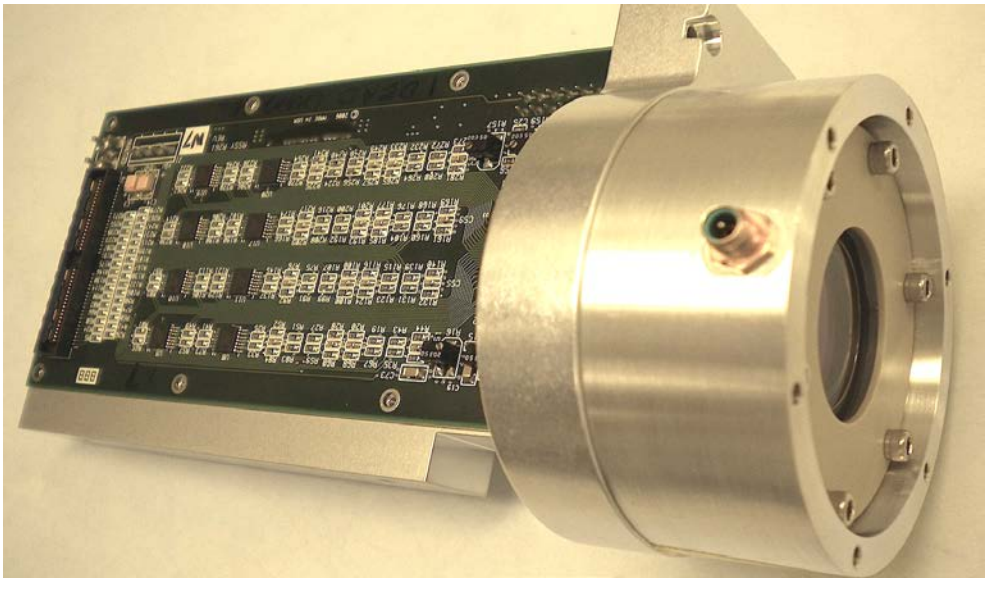

Fig. 7. RD20 amplifier board attached to 18mm sealed tube cross strip detector in housing.

The overall image response uniformity was assessed by illuminating the entire detector with a defocused laser beam (Fig. 11). The high statistics image (contrast enhanced) shows evidence of several effects. There is some residual banding in both X and Y which are attributable to centroid calculation errors for the individual strips and their associated amplifiers. In addition there is some fringing which is due to the laser input optical interactions with the entrance window. The former can be optimized by adjustment of the firmware algorithms for calculation of the

centroids. However, this fixed pattern noise is stable, and as is common in astronomical applications, flat field calibration data sets can be used to correct the non-uniformities, as has been done for the images shown in Fig. 19.

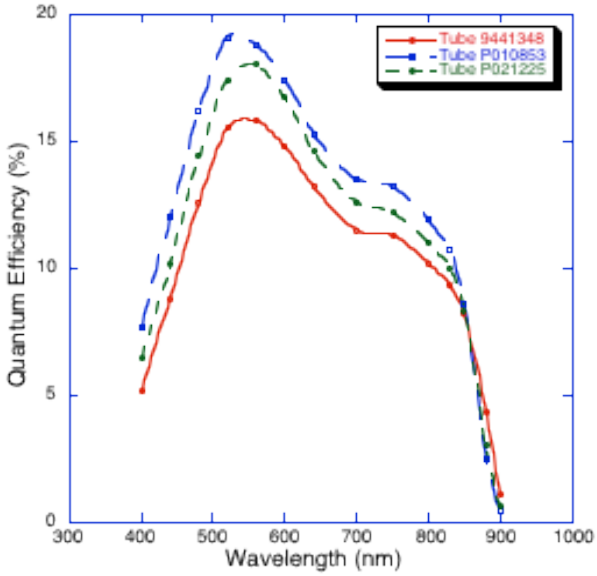

Fig. 8. Photocathode quantum efficiency for three 18 mm sealed tube cross strip anode detectors (SuperGen-II).

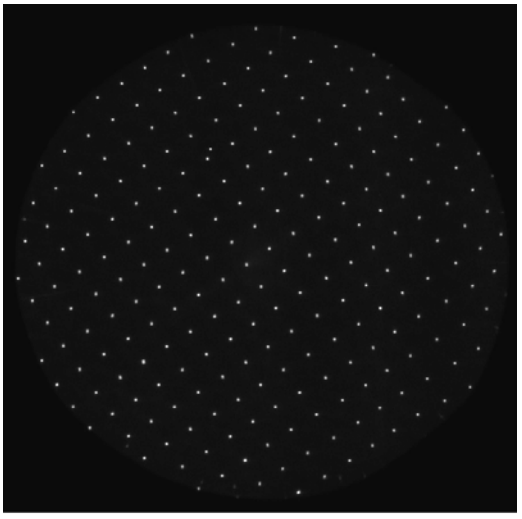

Fig. 9. Image of a projected 10 µm spot array on an 18 mm cross strip sensor. 1 mm x 1 mm spacings.

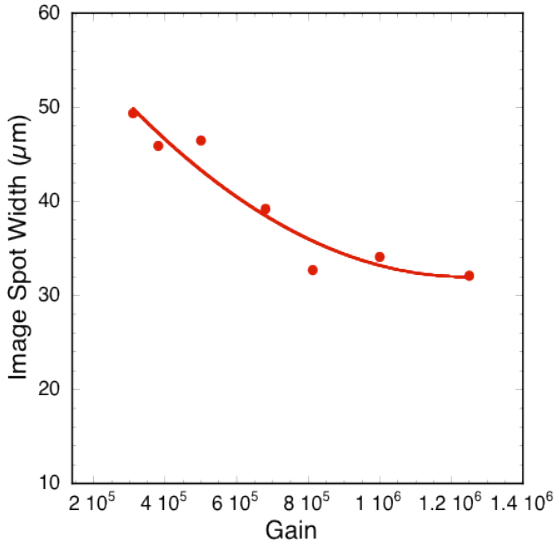

Fig. 10. Spatial resolution (FWHM) as a function of MCP gain, 18mm XS tube and PXS electronics. A limiting factor is the window to MCP proximity gap.

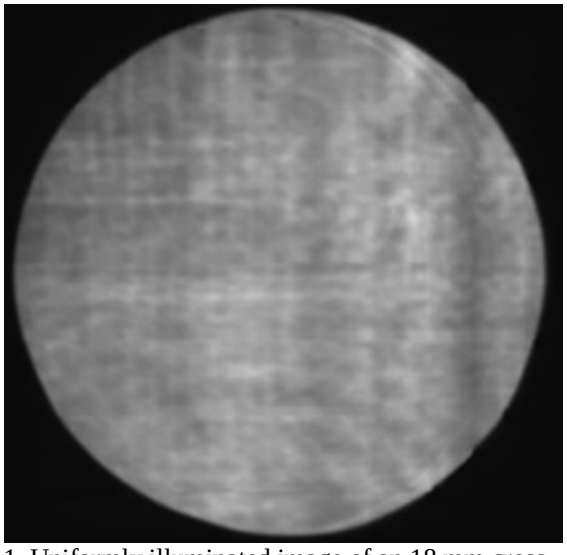

Fig. 11. Uniformly illuminated image of an 18 mm cross strip sensor (640nm Laser). Residual image modulations, due to individual strip amplifiers are stable and correctable.

2.5 Event Time Tagging

Various applications require timing information for each event detected [7, 8, 9, 10] and the demands of each vary. For astronomical applications this can be milliseconds for planetary transits or tens of microseconds for pulsars. Biological fluorescence lifetime and synchrotron time of flight instruments require as little as 100 ps and LIDAR can be of the same order. Time stamping of events using the FPGA clock frequency can establish event time resolution of ~10 ns with little difficulty. So along with the FPGA algorithms for X and Y position calculation we can establish a clock time for the event arrival time and add that to the data for the event. For more demanding timing applications there are a number of ways to establish better temporal resolution. MCP based detectors have the potential to be as good as ~25 ps, depending on the physical geometry, such as the proximity gaps, voltages, and MCP pore size. A traditional method to determine the time of arrival of the MCP exit pulse is an amplifier attached to the bottom of the MCP, and a constant fraction discriminator, and Time to Digital converter to compare the detected event time to the

pulse source input trigger. We have been able to do this for various detectors [8] and obtain ~100 ps time resolution, however in cases where the input trigger has a very high rate it can be difficult to implement. Since the MCP bottom contact has no position information it is unable to discriminate between closely temporally spaced events at different positions on the detector. A convenient method for establishing an event time can be derived from the anode signals, since these have been digitized on all anode strips and are available at the FPGA. In addition to calculating the event position centroid we can use a combination of the X and Y strip signal waveforms to make a "pulse" and determine its arrival time. This is achieved by constructing a firmware constant fraction discriminator applied to the derived "pulse" and interpolating the zero crossing point to a small fraction of the clock frequency. This method also allows spatially non-overlapping events that occur closely spaced in time to be processed.

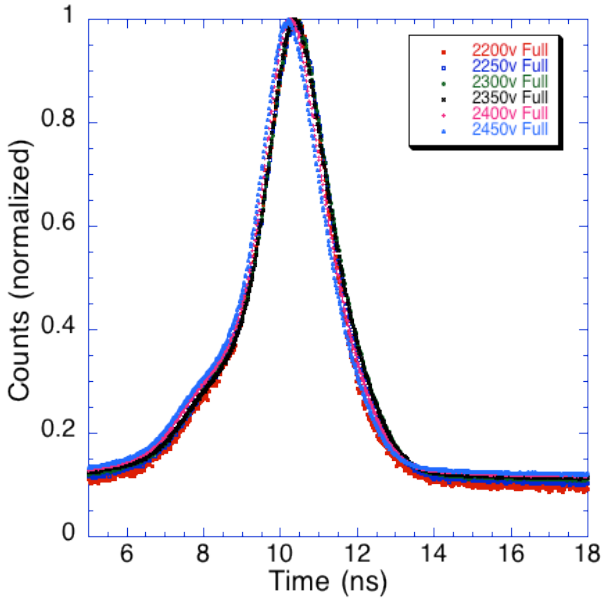

Fig.. 12. Event time stamp error distributions for an 18 mm cross strip sensor system as a function of MCP gain. Full sensor illumination with 640 nm laser. ~2ns error independent of gain is dominated by ~1.25 ns laser trigger jitter and amplifier pulse shape variations.

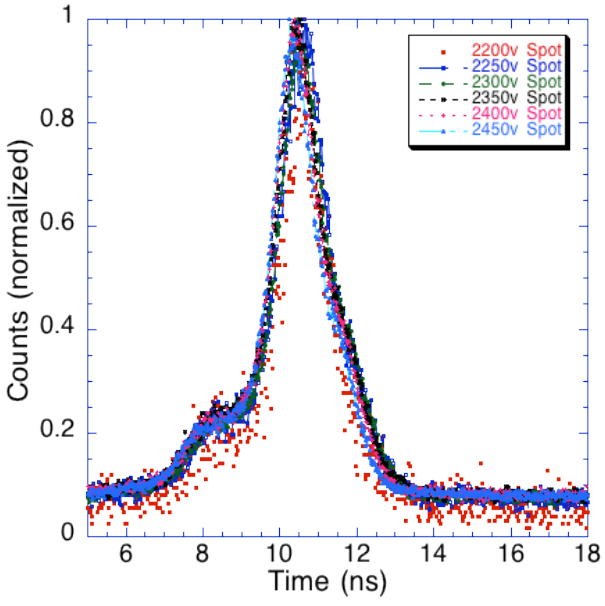

Fig. 13. Event time stamp error in a spot (<1 mm) as a function of event gain. 18 mm cross strip sensor system obtains ~1.25 ns FWHM dominated by laser trigger jitter.

Illuminating an 18mm cross strip sensor uniformly with 640 nm pulsed laser light (Fig. 12) shows that the resulting event timing jitter is about 2ns FWHM. This characteristic remains the same over a wide range of detector MCP gains, and does not improve as the signal to noise ratio increases. The same test, but using a small illuminated spot (1mm) gives a timing jitter of about 1.25 ns (Fig. 13), which is also independent of the signal to noise ratio. Further investigation has determined that the cause of the dominating component of this characteristic is the input trigger jitter of the laser itself (~ 1ns). The intrinsic accuracy of the cross strip system is probably much better than this and further tests to confirm this will be done with an improved laser source.

The difference between timing error distribution for the spot illumination case and the fully illuminated sensor has also been investigated. The average relative event arrival time as a function of position is shown in Fig. 14. We find that there are regions at the extremities of the X and Y axes, and several bands across each axis where temporal variations occur most. It should be noted that response of the RD20 amplifiers varies due to the capacitive load, with an increase in the pulse peaking time of about 1ns/pF of increased load. The strips at the axis extremes are the shortest (Fig. 2) and thus have the smallest capacitive load for the amplifiers. The band features have time variations of about 500ps, but the axis extremities are worse than this (Fig. 15). This suggests that timing spatial non-uniformities in Fig. 11 derive from small changes in the amplifier capacitive load due to the anode and other parasitics. So the uniformly illuminated time error distribution (Fig. 12) is actually the spot time error distribution (Fig. 13) folded with the spatial non-uniformities (Fig. 14) of the average arrival time. Both changes in amplifier design and anode structure could reduce this effect. However, note that the spatial variation in time tag is not a time jitter, but rather a fixed pattern timing offset that can be calibrated and applied to correct any data-set.

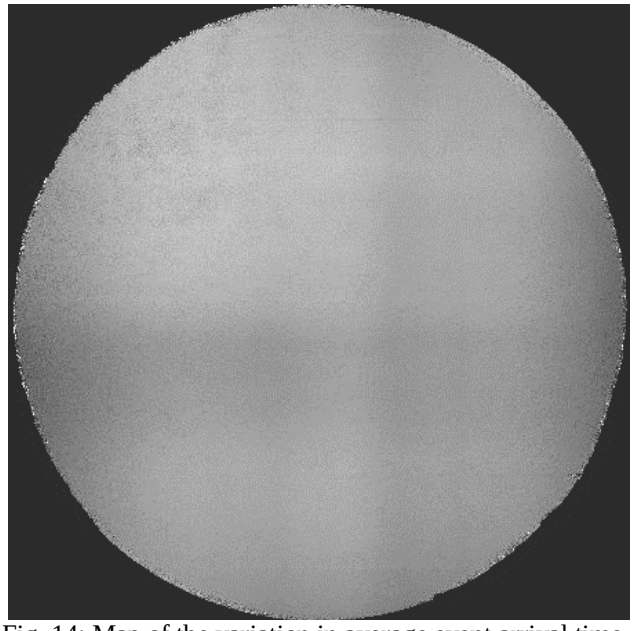

Fig. 14: Map of the variation in average event arrival time for an 18mm sealed tube cross strip detector system. This fixed pattern is stable and is correctable with a look up table.

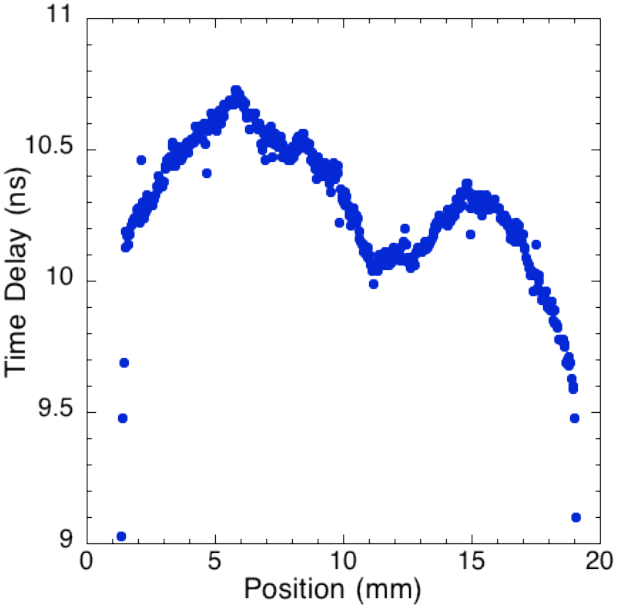

Fig. 15: Variation in the apparent mean arrival time of events v.s. position. From Fig. 14 along Y in the center of X.

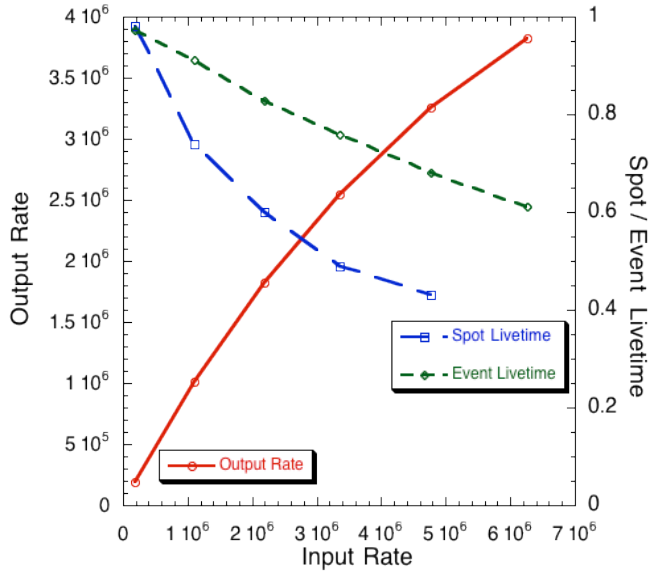

Fig. 16: Global event livetime (throughput) and unperturbed spot livetime vs. input count rate for an 18mm XS sensor. Spot image contrast is reduced at high rates due to the amplifier pulse decay time causing event pile-up misanalysis.

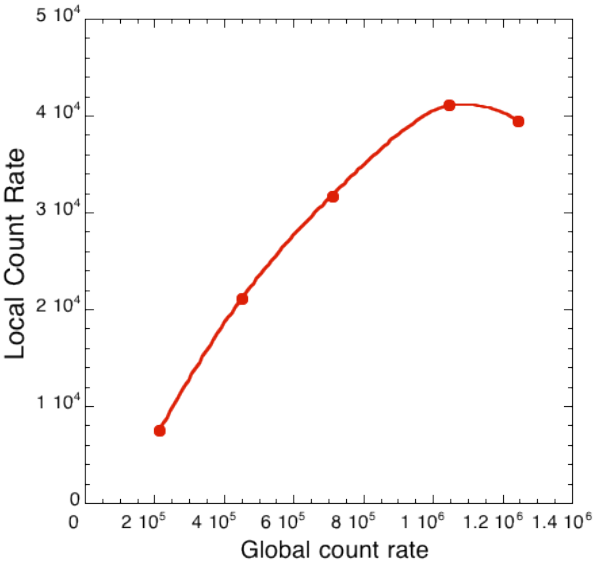

Fig. 17: Local (100 µm spot) event rate throughput for an 18mm XS sensor (90MΩ MCP stack). Achieves 40kHz before MCP recharge limit is reached.

2.6 Count Rate Throughput

The count rate throughput of a cross strip readout MCP detector is naturally separated into a global rate limit determined by the event processing electronics system, and a local rate limited by the MCP stack itself. In the PXS scheme, MCP output current pulses (~2 ns duration) are amplified in ASIC charge amplifiers (~40ns risetime, 250 ns falltime) and then converted to digital values at 50MHz by the ADC (20ns sampling). These are then parallel processed in an FPGA with all the other strip signals to produce spatial event centroids and temporal stamps in a downstream pipeline process before being transferred at high bandwidth to a PC interface. In theory, because of the parallel nature of the many strips samples, two events can be analyzed within three clock cycles (60 ns), as long as they do not overlap spatially. The three cycle limit (60ns) is due to our current slew rate thresholding scheme, where “valid” events are the events which have a difference between two sequential samples exceeding a set threshold. In practice, the output rate

versus input rate curve is best fit by an 80ns paralyzable deadtime (Fig. 16). The additional deadtime of 1 cycle is due to the fact that spatially overlapping events occurring within 60 ns are not detected by our slew rate trigger and thus are not recognized as independent events. An 80ns deadtime per event corresponds to a 67% event throughput at an input rate of 5 MHz.

Although events can get through the electronics at such high rates, they are often perturbed by neighboring events. Often, to achieve the best imaging performance, 7 or 9 strips may be used to calculate a spatial centroid. It does not take much signal in the wings (caused by a contemporaneous neighbor event) to displace an event a substantial distance from where it should have been mapped. When we measure a livetime throughput for an illuminated spot and only count the events that lie within the nominal spatial resolution, the effective throughput of *unperturbed* events is reduced (Fig. 16). We can apply pileup rejection algorithms to remove mis-analyzed events and increase the contrast. For the 22mm XS anode detector, we achieve a 44% livetime at 5MHz if we maintain the high contrast by pileup rejection. Currently the slower RD20 preamplifier ASIC recovery time is the limiting component to our high contrast high throughput imaging, and is a candidate for replacement with a faster preamplifier.

Unlike the global count rate throughput mentioned above, the local rate capability of an MCP detector is limited by the ability of the MCP pores to recharge electrically between events, which is both a function of the MCP resistance and the total charge gain of the MCP stack. For a given gain, an illuminated spot's output count rate will increase with the input rate until the local gain starts to sag. Eventually, some events output charge fall below the event electronic threshold and won't be counted. Fig 17 shows such a curve for a 22 mm cross strip sealed tube at a gain of ~5 x 10^5 where we varied the input spot rate for a 100 µm wide illumination spot on the detector. The highest local count rate achieved was ~42 kHz for this MCP pair resistance of 90 MΩ. The high rate limits are inversely proportional to gain, so can be increased by lowering the gain of the MCPs, but at the expense of spatial and temporal resolution which depend directly on signal amplitude, so optimizations are dependent on the requirements of the specific application.

3. DEMONSTRATION OF HIGH TIME RESOLUTION IMAGING PHOTON COUNTERS

The practical demonstration of a cross strip sealed tube sensor system can most easily be accomplished in several steps. In the early phases this is most conveniently done by imaging and time resolved imaging on astronomical objects. Although demonstrations on small telescopes are not likely to produce significant scientific data, they do permit the development of the processes needed to handle commissioning and setup, and understanding of the processes needed to acquire and analyze the data. To this end we have coupled an 18mm cross strip system to a 25cm telescope (Fig. 18) for

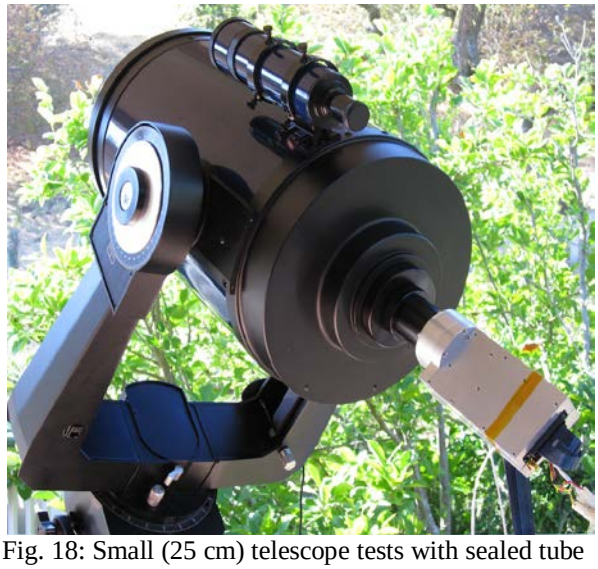

Fig. 18: Small (25 cm) telescope tests with sealed tube 18mm XS sensor (uncooled), as a testbed for imaging with photon event time tagging.

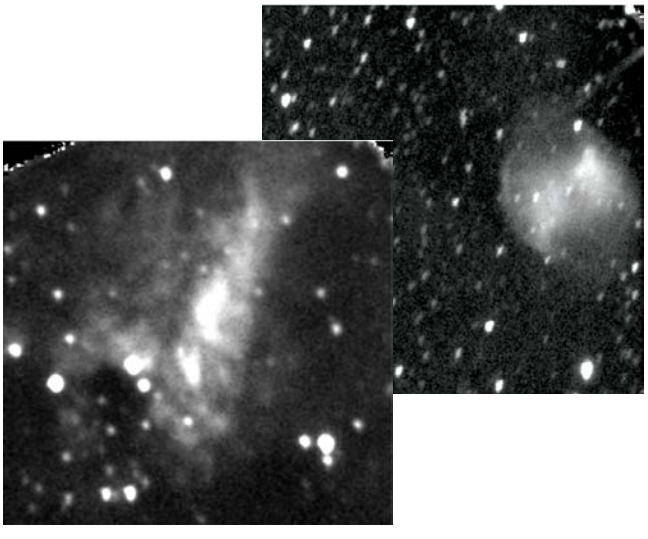

Fig. 19: The Omega Nebula (M17, left, 200sec) and the Dumbbell Nebula (M27, right, 400 sec) taken as tests with the system shown in Fig. 18.

tests in system commissioning. The overall hardware requirements are quite modest, comprising the XS detector and housing, PXS electronics, and high voltage and low voltage power supplies, along with a PC and data interface card. The overall sky background dominated observations with rates of the order 400 kHz. Despite some drift of the objects across the field of view, it was possible to use time resolved data to remap star positions and acquire images, that after flat field corrections give reasonable images of familiar objects (Fig. 19, M17 and M27). Further commissioning tests

will be done on other platforms to address applications in astronomy, night-time reconnaissance, biological single-molecule fluorescence lifetime microscopy and three dimensional imaging.

To underline the capabilities of high time resolution photon counting imaging we have commissioned an earlier generation of the detector, a sealed tube cross delay line sensor, at the Southern African Large Telescope, a 10m class instrument. In the process of making observations of astronomical variable sources we were also able to identify unrelated transients in our data sets. A typical case, such as the one shown in Figs. 20 and 21, is the detection of low brightness meteors. The meteor crossed the field of view in ~4 ms and had an extended ablation tail lasting ~ 10 ms. Binning our photon time tagged (25 ns) data into 100 μs frames we obtain a light curve (Fig. 21) and can construct a "movie" of the meteor crossing the field of view. The observation agrees well with existing data [20] of meteor altitudes and velocities for meteors brighter than $M_v = 5$, however it is much fainter than existing data sets achieve.

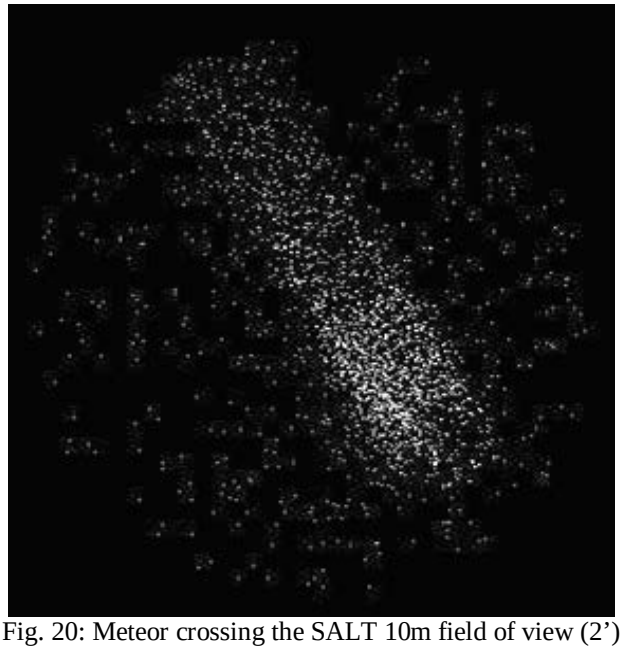

Fig. 20: Meteor crossing the SALT 10m field of view (2') showing the ablated head and tail (1 ms integration). [~10 km sec^{-1} at ~100 km] Equivalent magnitude ~9 M_v.

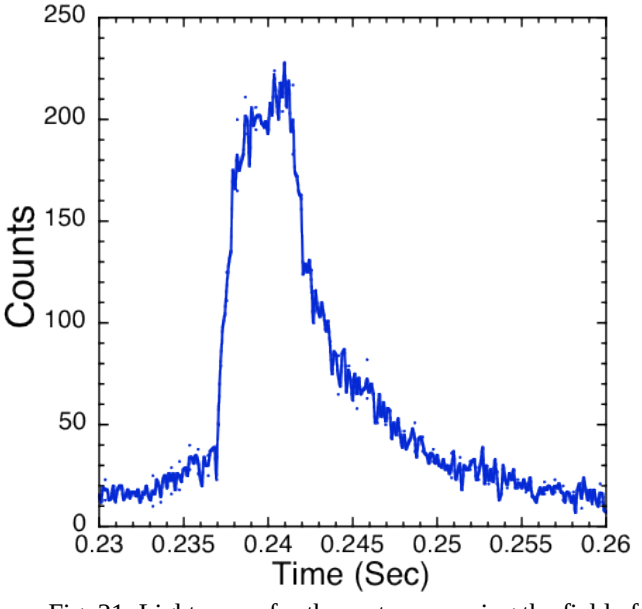

Fig. 21: Light curve for the meteor crossing the field of view showing the ingress of the head and decay of the tail (100 μs data bins).

4. ACKNOWLEDGEMENTS

We acknowledge the efforts of R. Raffanti, D. Rogers, J. Hull, D. Anderson, X. Michalet, R. Colyer, and our colleagues at SALT for their assistance in accomplishing these studies. This work was supported DOE grant #DE-FG52-08NA28773, and NSF grant #AST0352980. This report was prepared as an account of work sponsored by an agency of the United States Government. Neither the United States Government nor any agency thereof, or any of their employees, makes any warranty, expressed or implied, or assumes any legal liability or responsibility for the accuracy, completeness, or usefulness of any information, apparatus, product, or process disclosed, or represents that its use would not infringe privately owned rights. Reference herein to any specific commercial product, process, or service by trade name, trademark, manufacturer, or otherwise, does not necessarily constitute or imply its endorsement, recommendation, or favoring by the United States Government or any agency thereof. The views and opinions of authors expressed herein do not necessarily state or reflect those of the United States Government or any agency thereof.

5. REFERENCES

1. Siegmund, O.H.W., M.A. Gummin, J.M. Stock, et. al, Performance of the double delay line microchannel plate detect detectors for the Far-Ultraviolet-Spectroscopic Explorer, *Proc SPIE* 3114, pp.283-94, 1997.
2. Siegmund, O.H.W., P. Jelinsky, S. Jelinsky, et al., High resolution cross delay line detectors for the GALEX mission, *Proc. SPIE* 3765, pp.429-40, 1999.
3. Stock, J.M. O.H.W. Siegmund, J.S. Hull, et al.,Cross-delay-line microchannel plate detect detectors for the Spectrographic Imager on the IMAGE satellite, *Proc SPIE* 3445, pp.407-14, 1998.

4. Siegmund, O.H.W., M.A. Gummin, T. Sasseen, et al., Microchannel plates for the UVCS and SUMER instruments on the SOHO satellite, *Proc. SPIE* 2518, pp.334-55, 1995.
5. Vallerga, J.; Zaninovich, J.; Welsh, B.; Siegmund, O.; McPhate, J.; Hull, J.; Gaines, G.; Buzasi, D. The FUV detector for the cosmic origins spectrograph on the Hubble Space Telescope, *Nuclear Instruments and Methods in Physics Research Section A*, Volume 477, Issue 1-3, p. 551-555, 2002.
6. Siegmund, O.H.W., J. McPhate, A. Tremsin, J.V. Vallerga, B.Y. Welsh and J.M. Wheatley, *AIP Conference Proceedings*, 984, 103, 2008.
7. Priedhorsky. W.and J. Bloch, *Applied Optics*, 44(3), 423-433, 2004.
8. Siegmund, O.H.W., J. Vallerga, P. Jelinsky, M. Redfern, X. Michalet, S. Weiss, Cross Delay Line Detectors for High Time Resolution Astronomical Polarimetry and Biological Fluorescence Imaging, *IEEE* 2005 Nuclear Science Symposium and Medical Imaging Conference, Puerto Rico, October 2005.
9. Michalet, X.; Siegmund, O. H. W.; Vallerga, J. V.; Jelinsky, P.; Millaud, J. E.; Weiss, S., Photon-counting H33D detector for biological fluorescence imaging, Nuclear Instruments and Methods, A, Vol. 567(1), p. 133, 2006.
10. Tremsin, A.S., G.V. Lebedev, O.H.W. Siegmund, et al, High spatial and temporal resolution photon/electron counting detector for synchrotron radiation research, *Nucl. Instrum. and Meth. A*, 580, 853-857, 2006.
11. Berendse, F. B., R. G. Cruddace, M. P. Kowalski, D. J. Yentis, W. R. Hunter, G. G. Fritz, O. Siegmund, K. Heidemann, R. Lenke, A. Seifert, T. W. Barbee, Jr. The joint astrophysical plasmadynamic experiment extreme ultraviolet spectrometer: resolving power, Proc. SPIE Vol. 6266, 62660V, 2006.
12. Siegmund O.H.W., J.V. Vallerga, A. Martin, B. Feller, M. Arif. D. Hussey, and D. Jacobsen, A high spatial resolution event counting neutron detector using microchannel plates and cross delay line readout, *Nucl. Instr. & Meth. A*, 579, 188-191, 2006
13. Tremsin, A. S., O. H. W. Siegmund, J. V. Vallerga, J. Hull, *IEEE Trans. Nucl. Sci*. **51**, pp.1707-1711, 2004
14. Siegmund, O.H.W., A. Tremsin, J.V. Vallerga, J. McPhate, Microchannel plate cross strip detectors with high spatial and temporal resolution, Nucl Instrum Methods Phys Res A. 610(1), p.118, 2009.
15. Siegmund, O.H.W., Tremsin, Anton S., Vallerga, John V. Development of cross strip MCP detectors for UV and optical instruments, Proc. SPIE, Vol. 7435, p.14, 2009
16. Siegmund, O.H.W. John V. Vallerga, Anton S. Tremsin, Laura C. Stonehill, Robert Shirey, Michael W. Rabin, and David C. Thompson, Cross strip microchannel plate imaging photon counters with high time resolution, SPIE, Vol. 7681, p.768109, 2010.
17. Tremsin, A. S., J. V. Vallerga, O. H.W. Siegmund, J. S. Hull, "Centroiding algorithms and spatial resolution of photon counting detectors with cross strip anodes", Proc. SPIE, vol. 5164, pp.113-124 (2003).
18. Siegmund, O. H. W., A. S. Tremsin, J. V. Vallerga, R. Abiad and J. Hull, "High resolution cross strip anodes for photon counting detectors", Nucl. Instr. And Meth. **A 504** p177, 2003.
19. Haddad, K. C., H. Stark, N. P. Galatsanos, "Constrained FIR filter design by the method of vector space projections", IEEE Trans. Circuits and Systems II -Analog And Digital Signal Processing **47,** p 714, 2000.
20. Janches, D., M.C. Nolan, D.D. Meisel, J.D. Mathews Q.H. Zhou, and D.E. Moser, Journal of Geophysical Research, Vol. 108, No. A6, p1222, 2003.